

Strong electron-phonon coupling in the rare-earth carbide superconductor La_2C_3

J. S. Kim, W.-H. Xie, R. K. Kremer, V. Babizhetskyy, O. Jepsen, and A. Simon
Max-Planck-Institut für Festkörperforschung, Heisenbergstraße 1, 70569 Stuttgart, Germany

K. S. Ahn

Department of Chemistry, Yonsei University, Wonju 220-710, South Korea

B. Raquet, H. Rakoto, and J.-M. Broto
*Laboratoire National des Champs Magnétiques Pulsés,
143 avenue de Rangueil, 31432 Toulouse, France*

B. Ouladdiaf

Institute Laue-Langevin, Grenoble, Cedex 9, France

(Dated: September 18, 2018)

We present the results of a crystal structure determination using neutron powder diffraction as well as the superconducting properties of the rare-earth sesquicarbide La_2C_3 ($T_c \approx 13.4$ K) by means of specific heat and upper critical field measurements. From the detailed analysis of the specific heat and a comparison with *ab-initio* electronic structure calculations, a quantitative estimate of the electron-phonon coupling strength and the logarithmic average phonon frequency is made. The electron-phonon coupling constant is determined to $\lambda_{ph} \sim 1.35$. The electron-phonon coupling to low energy phonon modes is found to be the leading mechanism for the superconductivity. Our results suggest that La_2C_3 is in the strong coupling regime, and the relevant phonon modes are La-related rather than C-C stretching modes. The upper critical field shows a clear enhancement with respect to the Werthamer-Helfand-Hohenberg prediction, consistent with strong electron-phonon coupling. Possible effects on the superconducting properties due to the non-centrosymmetry of the crystal structure are discussed.

PACS numbers: 74.25.Bt, 74.25.Jb, 74.70.Ad, 74.62.Bf

I. INTRODUCTION

The recent discovery of superconductivity in MgB_2 ¹ and alkaline earth-intercalated graphites² as well as Li at high pressures^{3,4} has renewed the interest in electron-phonon (*e-ph*) coupled superconductors without strong electron-electron correlations. The electronic states and phonon modes relevant for superconductivity vary from system to system, but in general superconductivity in these compounds benefits from the light atomic mass of constituents *e.g.* of boron, carbon and lithium. When a specific part of the Fermi surface (FS) couples strongly to high frequency phonon modes, an increase of T_c can be achieved even if the *e-ph* coupling averaged over the full FS remains moderate. This mechanism opens a new route to achieve high T_c 's by *e-ph* pairing.⁵ This is often associated as the "metallic hydrogen superconductivity" scenario.⁶

The rare earth sesquicarbides, $R_2\text{C}_3$ (R = Rare earths), which crystallize in the bcc Pu_2C_3 structure-type, have been suggested as possible candidates, in which such conditions are realized. Early on, T_c of La_2C_3 and Y_2C_3 was found to be ~ 11 K, and Th doping in Y_2C_3 raises T_c to 17 K,⁷ comparable with the T_c 's of the A15 compounds. In the Pu_2C_3 structure, C_2 dumbbells are located inside the rare earth metal atom cage. Since the C-C bond is quite short, the phonon frequency for the C-C stretching phonon modes is expected to be

very high. In fact, recent *ab-initio* calculations showed that the C-C stretching phonon frequency in Y_2C_3 is $\sim 1442 \text{ cm}^{-1}$.⁸ Therefore *e-ph* coupling between the high frequency phonons and C-C antibonding states at the Fermi level (E_F) has been considered as an origin of the relatively high T_c in Y_2C_3 and La_2C_3 .

Superconductivity in rare earth sesquicarbides recently regained attention because of the discovery of 18 K superconductivity in Y_2C_3 samples prepared under high pressure (~ 5 GPa).^{9,10} The upper critical field (H_{c2}) is also significantly increased and amounts to $H_{c2}(0) > 30$ T.⁹ Electronic structure calculations^{8,11} for Y_2C_3 , however, demonstrated that the high frequency C-C bond stretching phonon modes contribute less than 10% of the total *e-ph* coupling, and rather low frequency Y(-C) phonons must be considered to be the relevant modes for superconductivity. For stoichiometric band filling, the *e-ph* coupling constant λ_{ph} is predicted to be ≈ 0.6 . These results were consistent with previous H_{c2} studies on La_2C_3 , which reported $\lambda_{ph} \sim 0.8$ suggesting moderate *e-ph* coupling.¹² However, such a moderate *e-ph* coupling appears to be too small to generate the relatively high T_c in the sesquicarbide superconductors.⁸ Therefore, to reconcile with the measured T_c , it is necessary to consider either significant *e-ph* coupling with the high frequency C-C stretching phonon modes or strong *e-ph* coupling with the low frequency rare earth related phonon modes. In order to shed light on this controversy, further exper-

imental studies on the superconducting properties of the R_2C_3 are required.

In this paper we focus on one of the rare earth sesquicarbides, La_2C_3 . We investigate its superconducting properties together with the crystal and electronic structures. In the rare earth sesquicarbides, it has been well known that T_c as well as the structural properties vary significantly depending on the synthesis and annealing conditions, essentially due to C deficiency. Therefore in order to carry out reliable studies on such compounds, one needs to characterize the superconducting properties simultaneously with the structural properties with particular attention to C deficiency. Unlike Y_2C_3 , which requires high pressure and high temperature preparation, La_2C_3 can be prepared at ambient pressure conditions using standard arc melting technique, and larger sample quantities can easily be synthesized. Recently, we reported that T_c of La_2C_3 can be enhanced up to 13.4 K using excess C in the starting composition of the materials combined with an adequate post-annealing.^{13,14,15,16,17}

In addition, La_2C_3 can be a potential system for investigating the effect of non-centrosymmetry in the structure. The space group symmetry of R_2C_3 , $I\bar{4}3d$, belongs to the tetrahedral crystallographic class T_d lacking a center of symmetry. When the crystal structure has no center of symmetry and spin-orbit coupling is significant, the degenerate spin-up and spin-down bands are mixed and split, which can induce unexpected superconducting properties. For example, one of the well-known non-centrosymmetric superconductors $CePt_3Si$,¹⁸ where Ce f -bands possess significant spin-orbit coupling,¹⁹ shows unconventional superconducting properties such as high $H_{c2}(0)$ exceeding the Pauli limit¹⁸ and a line node in the superconducting order parameter.^{20,21} However, this system also shows a heavy fermion nature, and it is not clear yet how far the origin of the exotic properties has to be attributed to the non-centrosymmetry. Thus, it is required to explore other non-centrosymmetric superconductors *without* strong electron correlations.²² In this respect, R_2C_3 compounds with non-magnetic rare earths, can also be such model compounds to study only the effect of the non-centrosymmetric structure without the interference from the magnetism of the constituents.²³ In case of Y_2C_3 , the spin-orbit coupling for Y d -bands may be rather small, thus we can not expect a significant effect of non-centrosymmetry. Because of the higher atomic mass of La as compared to Y, spin-orbit coupling effects in La_2C_3 is expected to be more pronounced than in Y_2C_3 . Note that La is placed next to Ce in the periodic table and accordingly is expected to generate comparable spin-orbit coupling.

The paper is organized as follows; we first provide experimental details including a brief description on the synthesis procedures (Sec. II). Secondly we discuss the crystal structure at low temperatures gained from neutron powder diffraction (NPD) investigations (Sec. III) and report the electronic structures of La_2C_3 obtained from *ab-initio* calculations (Sec. IV). Specific heat (Sec.

V) and the upper critical fields (Sec. VI) on the samples characterized by NPD are presented. Finally we will discuss the e - ph coupling strength of La_2C_3 and also the effects of non-centrosymmetry on the superconducting properties (Sec. VII).

II. EXPERIMENTAL

Polycrystalline samples of La_2C_3 were synthesized by arc melting the constituents on a water-cooled Cu crucible under purified Ar atmosphere. La metal chips (Ames Laboratory, 99.99%) were used with spectroscopic grade graphite chips (Deutsche Carbone, 99.99%). Before use, the graphite chips were outgassed overnight at 950 °C under high vacuum conditions ($P < 10^{-5}$ mbar). The starting materials were melted more than 6 times and at each time the button was turned over to ensure homogeneity. La_2C_3 is very moisture-sensitive, tending to decompose readily within a few minutes on exposure to the air. Consequently all handling of the starting materials and the samples after synthesis was performed in an Ar filled glove box (M. Braun $P_{H_2O} < 0.1$ ppm).

It has been reported that a homogeneity range exists for La_2C_3 extending from 45.2% to 60.2% atom-% C content.²⁴ After investigation of a series of $La_2C_{3-\delta}$ samples,^{13,15,16} it was concluded that samples with a carbon deficit upon annealing phase separate into two superconducting phases with rather sharp T_c 's of ~ 6 K and 13.4 K. The latter transition which can be attributed to the almost stoichiometric La_2C_3 phase, is significantly higher than the T_c of ~ 11 K reported so far for La_2C_3 . Therefore, to obtain samples with a single sharp superconducting transition at 13.4 K, it is essential to compensate possible losses of C in the arc melting and the subsequent annealing procedure by an excess of carbon up to 10%, although this may result in the impurity phase which is identified to be LaC_2 . Heat treatment of the sample buttons was performed in sealed Ta tubes under purified Ar atmosphere at 1000°C. After annealing at high temperatures, the samples were slowly cooled to room temperature with a rate of 5°C/hour.

Neutron powder diffraction experiments on 2 samples of La_2C_3 (samples, S1 and S2, *cf.* Table I) were performed at room temperature using the GEM diffractometer at the ISIS laboratory. For low temperature neutron powder experiments, another La_2C_3 sample (sample S3) of ≈ 10 g was sealed into a vanadium can under 1 bar of He gas and measured down to 5 K on the D2B diffractometer at the Institut Laue-Langevin (ILL). The structural parameters as well as the La_2C_3/LaC_2 composition were gained from two-phase Rietveld refinements using the FULLPROF package.²⁵ T_c was determined from dc magnetic susceptibility measurements using a SQUID magnetometer (Quantum Design, MPMS XL magnetometer). The specific heat (C_p) was measured using a PPMS calorimeter (Quantum Design) employing the relaxation method. The C_p contribution from the

LaC₂ impurity phase was estimated from the results of a separate run on a pure LaC₂ sample characterized also with neutron powder diffraction. To determine the upper critical fields, we measured the temperature dependence of the resistivity for a bar shape sample ($1 \times 1 \times 5 \text{ mm}^2$) of La₂C₃ at different magnetic fields up to 11 T. For magnetic fields higher than 11 T, we performed magnetization and resistivity measurements in a pulsed magnetic field up to 30 T at the Laboratoire National des Champs Magnétiques Pulsés in Toulouse.

III. NEUTRON POWDER DIFFRACTION

La₂C₃ crystallizes with the cubic Pu₂C₃ structure (I43d) with 8 formula units in the unit cell. As shown in Fig. 1, C-C dumbbells are located in a distorted dodecahedral coordination ('bisphenoid') formed by 8 La atoms. So far, several crystal structure determinations for La₂C₃ have been carried out by neutron powder diffraction^{26,27} and also by x-ray single crystal diffraction.¹⁵ There was some variation found for the lattice parameters ranging from $a = 8.804$ to 8.818 \AA at room temperature.^{26,27,28} Such a wide spread of structural parameters has been already known for Y₂C₃⁹ as well as other C-containing superconductors like MgCNi₃.²⁹ It is related to the C

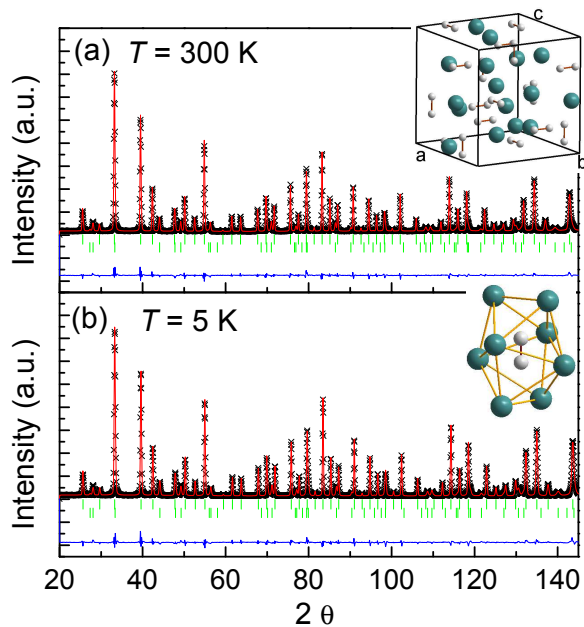


FIG. 1: (Color online) Neutron powder diffraction patterns of La₂C₃ (S3) at (a) 300 K and (b) 5 K (D2B, ILL). The (red) solid line represents the Rietveld refinement. The difference between the observed data and the calculated curve is shown at the bottoms while the Bragg positions are indicated by upper and lower bars for La₂C₃ and LaC₂, respectively. The crystal structure of La₂C₃ and the C-C dumbbell structure surrounded by the La cage (bisphenoids) are shown in the insets of (a) and (b), respectively. Large (small) spheres denote La (C).

content and often affects the superconducting properties quite substantially. For example, in MgC_xNi₃, the density of state at E_F , $N(E_F)$, decreases rather abruptly due to disorder-induced smearing of the electronic bands.³⁰ In addition, e - ph coupling mostly due to the low energy Ni-dominated phonon modes is reduced by C deficiency.^{31,32} Similar effects of C deficiency may also cause the large variations of superconducting properties in R_2C_3 compounds.

Figure 1 shows the neutron powder diffraction patterns of La₂C₃ (S3) collected at $T = 300 \text{ K}$ and 5 K . In addition to the reflections which can be ascribed to La₂C₃, there are extra weak reflections, which belong to the impurity phase, identified as LaC₂ (I4/mmm). A two-phase Rietveld refinement was performed to account for the admixture of the LaC₂ phase whose weight fraction is refined to $\approx 18\%$. The converged parameters of the La₂C₃ phase include the lattice constants, the fractional coordinates $(u, u, u)_{La}$ of the La 16c site and $(v, 0, 1/4)_C$ of the C 24d sites, an isotropic (anisotropic) thermal parameters for the La (C) sites. After refinements with the aforementioned parameters, in a last step, the C occupancy was varied. We checked convergence by varying the C occupancy in the cases where the other refined parameters are fixed or relaxed. For both cases, a C deficiency of $\sim 2\%$ is derived consistently. The results of the refinements for the two patterns collected at $T = 300 \text{ K} - 5 \text{ K}$ are listed in Table I. Also the results for samples S1 and S2 obtained using time-of-flight (TOF) patterns collected at room temperature are given.

The C-C distance at room temperature amounts to $\approx 1.295 \text{ \AA}$, in agreement with the previously reported value, $1.296(9) \text{ \AA}$ [Ref. 27] but smaller than that reported early on, 1.32 \AA .²⁶ Similar C-C distances have also been observed in binary rare earth dicarbides and ternary carbide halides.^{33,34,35,36} From the studies of electronic behavior on a series of the dicarbides, MC_2 , the C-C bond length inside the octahedral metal atom cage is found to be linked to the valence state of the M atoms.³⁶ In a simple ionic picture, CaC₂ ($Ca^{2+}(C_2)^{2-}$) with filled bonding π states but empty antibonding π^* and σ^* states, has a short C-C bond distance of $\approx 1.2 \text{ \AA}$, while with increasing electron count for the C₂ unit *e.g.* in UC₂ ($U^{4+}(C_2)^{4-}$), the C-C bond distance increases to $\approx 1.35 \text{ \AA}$ as the antibonding π^* states are gradually filled. La₂C₃ has a shorter C-C bond in a C_2^{4-} unit, which is presumably due to the different degree of charge transfer to antibonding C-C π^* states. These results indicate that the charge transfer between M states and antibonding π^* state of the C-C dimers strongly depends not only on the valence state of M , but also the local environment around the C-C dimers because of different cage structure.

Interestingly we observed a significant temperature dependence of the C atom position in contrast to that of the metal atom cage which contracts in a regular way. With decreasing temperature a slight increase of the C-C bond distance is found (see Table I). A possible explanation of this observation could be a temperature dependence

TABLE I: Structural parameters for La_2C_3 obtained from Rietveld refinements of neutron powder diffraction patterns at $T = 300$ K (S1-S3) and at low temperature down to 5 K (S3). a is the cubic lattice parameter and $d_{\text{C-C}}$ is the C-C bond length. u and v are the fractional coordinates of the La $16c$ site $(u, u, u)_{\text{La}}$ and the C $24d$ sites $(v, 0, 1/4)_{\text{C}}$, respectively. The reduced χ^2 , the occupancy for C are listed. The employed method, time-of-flight (TOF) and constant-wavelength (CW) neutron powder diffraction is also indicated.

Sample	T (K)	a (Å)	u (La)	v (C)	χ^2	$d_{\text{C-C}}$ (Å)	C occupancy	Method
S1	300	8.80991(8)	0.05255(3)	0.30155(9)	2.074	1.2942(16)	0.983(8)	TOF
S2	300	8.8090(1)	0.05268(6)	0.30171(16)	1.325	1.2911(28)	0.977(5)	TOF
S3	300	8.8096(3)	0.05255(6)	0.30144(14)	8.96	1.2977(19)	0.982(2)	CW
	200	8.8013(3)	0.05251(5)	0.30114(14)	9.42	1.3001(17)		CW
	100	8.7936(3)	0.05251(5)	0.30085(13)	10.06	1.3041(17)		CW
	5	8.7904(3)	0.05250(5)	0.30065(13)	10.29	1.3071(17)		CW

of the charge transfer between the C-C π^* to the La d states. A carbon-metal orbital overlap will be affected by volume contraction at low temperatures, which will modulate the charge transfer between La d and C-C π^* states. Another possible origin could be a tilting motion of the C-C dimers leading to unusual non-elliptical temperature factors which can not be accounted for by the refinement procedure. Further studies are ongoing to clarify this issue.

IV. ELECTRONIC STRUCTURE CALCULATIONS

The electronic structure of La_2C_3 has been studied using the full-potential linear augmented plane wave (LAPW) method with local orbital extension, within the generalized gradient approximation (GGA).^{37,38,39} We performed total-energy calculations for a series of the lattice parameters. For each lattice parameter the internal parameters (atomic positions) were relaxed according to the atomic forces. By this procedure, the fully relaxed structural parameters have been obtained including the lattice constant as well as the La and C atomic positions. The calculated equilibrium lattice constant is $a = 8.829$ Å, with a C-C distance of 1.333 Å and a La-C distance of 2.709 Å, corresponding to internal parameters, $u_{\text{La}} = 0.0524$ and $v_{\text{C}} = 0.2995$. In comparison with the Rietveld refinement results at 5 K, the calculated lattice parameter is within the normal error bar of LAPW calculations ($\sim 1\%$), while the internal atomic parameters for both La and C are in good agreement.

Figure 2 displays the electronic structure with and without spin-orbit coupling included, using the optimized structural parameters. There are 6 C-C dimers in the primitive cell, and the orbitals on these form bonding and antibonding C-C π - π^* bands. The C $2s$ derived bands extend from -15.6 eV to -6.2 eV, relative to the Fermi energy. The lowest bands around -14 eV and the bands around -7.5 eV are the bonding and antibonding states, respectively. The bands around -4 eV are the bonding carbon p bands. The bands crossing the Fermi level, separated by a 2.5 eV gap from the bonding C-C π bands, are the hybridized La d and C-C antibonding π^* states.

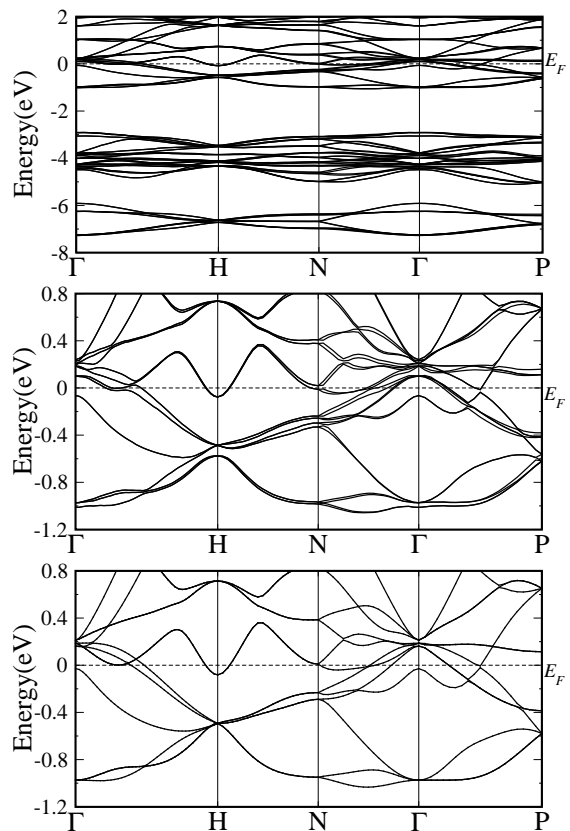


FIG. 2: *Upper panel*: Calculated band structure of La_2C_3 with spin-orbit coupling, using the theoretical lattice constant with fully relaxed atomic positions. For comparison, the band structures near E_F with (*middle panel*) and without (*bottom panel*) spin-orbit coupling are also presented.

The electronic structure obtained including spin-orbit coupling is quite similar to that without spin-orbit coupling, except that the number of bands is doubled due to the asymmetric spin-orbit coupling effect (See middle and bottom panels in Fig. 2). Lacking inversion symmetry in the structure along with significant spin-orbit coupling, some spin-up and spin-down bands are mixed and the degeneracy is lifted. Therefore, in contrast to the previous conjecture,⁴⁰ the band splittings due to the asymmetric spin-orbit coupling do exist, and may also affect the superconducting properties. In particular, for La_2C_3 , relatively flat bands are crossing E_F , thus such a band splitting may alter significantly the total electronic density of states (DOS) at E_F . In Fig. 3, we show the DOS with and without spin-orbit coupling around E_F . The DOS near the Fermi level is characterized by a broad minimum centered at about 50 meV below E_F . As shown in the inset of Fig. 3, for stoichiometric compounds $N(E_F)$ is reduced by $\sim 10\%$ by introducing the spin-orbit coupling.

We also calculated the DOS for the system with 2% C deficiency by employing the virtual-crystal approximation. We noticed a shift of peaks towards higher energies above E_F . As seen in Fig. 3, while the electronic structure based on the stoichiometric sample puts E_F on the shoulder of the peak located near the Fermi level, E_F for the 2% C deficient sample lies close to a minimum. This leads to a reduction of $N(E_F)$ by $\sim 25\%$ as compared to the DOS based on the stoichiometric La_2C_3 assuming no spin-orbit coupling. Introducing the spin-orbit coupling, the reduction of $N(E_F)$ is even more pronounced and amounts to $\sim 30\%$. Thus slight C deficiency can significantly change the electronic properties. This provides an explanation of the strong dependence of T_c and the upper critical field on the composition found in Y_2C_3 and La_2C_3 .^{9,10,13,14,15,16}

Singh and Mazin concluded that λ_{ph} has a maximum at the stoichiometric band filling.⁸ This is closely related

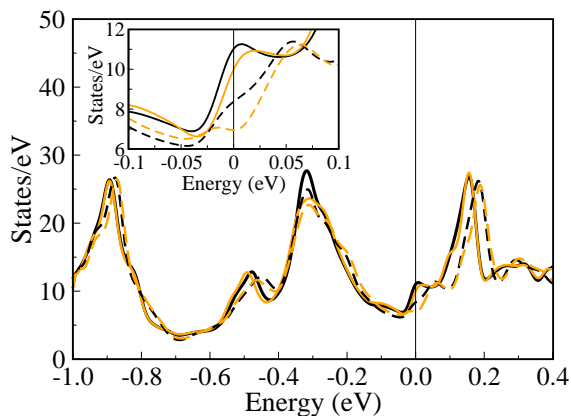


FIG. 3: (Color online) Electronic density of states of La_2C_3 without (black) and with (yellow) spin-orbit coupling for the stoichiometric (solid) and 2% C-deficient (dashed) compounds. The inset shows the DOS near the Fermi level.

to the observation that the Fermi energy falls on a peak in the electronic density of states. Hence, $T_c \approx 13.4$ K in the present 2% C deficient La_2C_3 samples is already higher than the previously known $T_c \sim 11$ K, but it seems that there is still a possibility to increase T_c further for stoichiometric La_2C_3 . In this view, the doping dependence of T_c for La_2C_3 can also be understood. Th doping in La_2C_3 enhances T_c up to 14.3 K,⁴¹ while Lu or Y doping slightly decreases T_c .²⁸ Considering the electron count for Th, Th doping at the La sites will donate more electrons than La, in contrast to Y or Lu substitution. For the previously investigated La_2C_3 samples ($T_c \sim 11$ K), the reduced electron concentration due to C deficiency, is compensated by Th doping, but not by Lu or Y doping. Therefore, enhancement of T_c by Th doping can be attributed to the recovery of the band filling towards the stoichiometric value.

V. SPECIFIC HEAT

Figure 4 shows the temperature dependence of the specific heat of La_2C_3 (S1) at $H = 0$ and $H = 9$ T. The contribution of LaC_2 to the total sample capacity, which amounts to $\lesssim 5\%$ over the whole temperature range, was subtracted. Note that T_c of LaC_2 is $\lesssim 1.6$ K,^{42,43} below the temperature range of the present measurements. There is no offset of C_p/T at $H = 0$ as the temperature approaches zero as can be seen in the inset of Fig. 4. This proves that the C_p contribution from the non-superconducting part, LaC_2 has been completely accounted for the subtraction. A sharp anomaly at ≈ 13.4 K is clearly resolved indicating bulk superconductivity in the La_2C_3 sample, which has not been observed

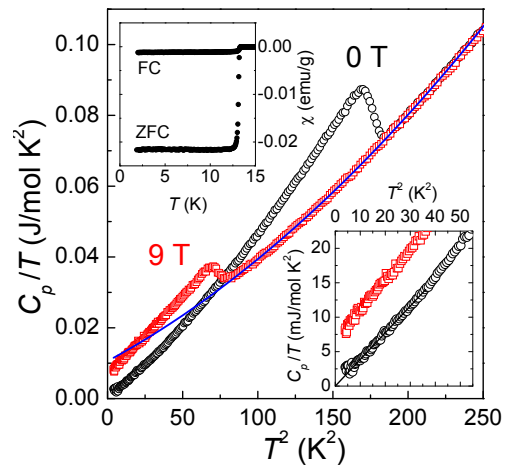


FIG. 4: (Color online) Temperature dependence of the specific heat of La_2C_3 at $H = 0$ and 9 T. The solid (black) line through the data points at $H = 9$ T (also in the right inset) is a fit described in the text. The insets show the low temperature behavior of $C_p(T)/T$ and the magnetic susceptibility with zero-field cooled (ZFC) and field-cooled (FC) modes.

previously.⁴⁴ The onset of 13.4 K determined from the specific heat jump is consistent with that obtained from the susceptibility measurements. At $H = 9$ T, the superconducting anomaly is shifted to lower temperatures. A clear deviation from a Debye T^3 law is observed in the normal state C_p , which can be attributed to a contribution from low-lying Einstein phonon modes.⁴⁵

In order to account for the normal state C_p , we fitted the data obtained at $H = 9$ T by a polynomial,

$$C_p(T) = \gamma_N T + C_{lattice}(T) = \gamma_N T + \beta T^3 + \delta T^5. \quad (1)$$

Here, γ_N is the Sommerfeld coefficient and β is related to the Debye temperature $\Theta_D(0)$ via

$$\Theta_D^3(0) [\text{K}] = 1944n/\beta [\text{J/molK}^4], \quad (2)$$

where n is the number of atoms per formula unit. Since the applied magnetic field $H = 9$ T is not sufficient to suppress superconductivity completely, we used a constraint according to

$$\int_0^{T_c} C_p(T)/T dT = \int_0^{T_c} (\gamma_N + \beta T^2 + \delta T^4) dT, \quad (3)$$

to assure the entropy conservation for the superconducting state.

The solid line in Fig. 4 is the best fit to the $H = 9$ T data for $T_c(H = 9 \text{ T}) < T < 15$ K, yielding the parameters, $\gamma_N = 10.60(4)$ mJ/mol K², $\beta = 228.2(11)$ $\mu\text{J/mol K}^4$, and $\delta = 0.5988$ $\mu\text{J/mol K}^6$. The measured γ_N is much higher and more realistic than those previously reported from specific heat⁴⁴ and upper critical fields measurements.¹² The corresponding Debye temperature

$\Theta_D(0) = 349(1)$ K is comparable with that found in previous work.⁴⁴

The specific heat difference $\Delta C_p(T)/T$ between the normal and superconducting state and the entropy for the superconducting state is shown in Fig. 5. For comparison, we also plot the BCS curve for the weak e - ph coupling limit. A clear deviation from the BCS curve is observed. The C_p anomaly at T_c as well as the intersection temperature where $\Delta C_p/T = 0$ is much higher than expected from the BCS prediction. The solid (red) line is the theoretical fit based on the ‘ α -model’ assuming an isotropic s -wave BCS gap $\Delta(T)$ scaled by the adjustable parameter, $\alpha = \Delta(0)/k_B T_c$.⁴⁶ For the weak coupling limit α is 1.76. The detailed temperature dependence of $\Delta C_p/T$ was fitted by two adjustable parameters: α and the Sommerfeld coefficient γ_N . The data are very well reproduced by $\alpha = 2.43$ and $\gamma_N = 8.97$ mJ/mol K². The γ_N value from the α model fit is slightly smaller than obtained from the normal state C_p , but in view of the experimental resolution and the accuracy of the model, it can be considered as satisfactory agreement. The normalized specific heat jump, $\Delta C_p/\gamma_N T_c$ is also higher than the weak limit BCS value, 1.426 giving a clear indication for an enhanced e - ph coupling.

The normalized electronic specific heat, $C_{es}/\gamma_N T_c$ in the superconducting state is shown in Fig. 6. The solid line is an exponential fit to the data for $2.0 \leq T_c/T \leq 4.5$ using the form $C_{es}/\gamma_N T_c \propto \exp(-0.82\alpha T_c/T)$ with $\alpha = 2.31(5)$. C_{es} exponentially vanishes for $T \rightarrow 0$ K, clearly manifesting the absence of gap nodes in the superconducting order parameter. The α value is somewhat lower than found from the α -model fit in which the ratio $\Delta(0)/k_B T_c$ is largely determined by the shape of the

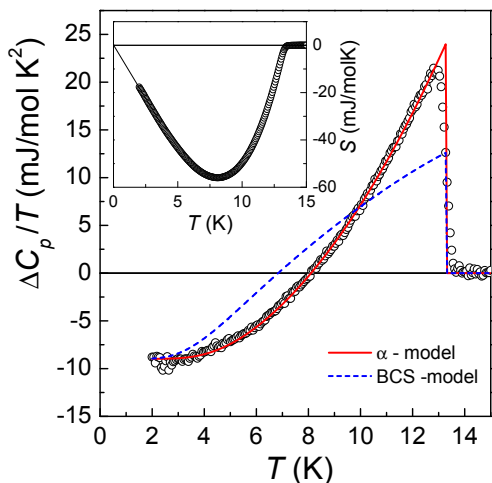


FIG. 5: (Color online) Superconducting part of the electronic specific heat. The (red) solid line is the best fit according to the α -model assuming an isotropic s -wave BCS gap as described in the text. The (blue) dashed line represents the BCS result. The inset shows the entropy conservation for the electronic specific heat in the superconducting state.

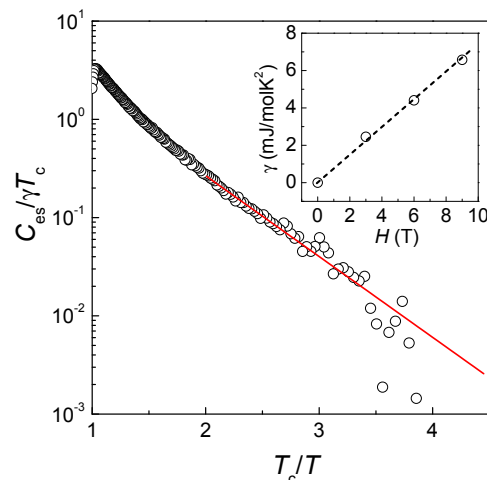


FIG. 6: (Color online) The electronic contribution of the specific heat C_{es} is plotted on a logarithmic scale versus T_c/T . The (red) straight line is an exponential fit for $2.0 < T_c/T < 4.5$. The magnetic field dependence of Sommerfeld coefficient $\gamma(H)$ is presented in the inset with the dashed line as a guide to the eye.

C_p jump near T_c . However the discrepancy is less than 10%, which is probably due to a restricted temperature range. The magnetic field dependence of $\gamma(H)$ at $T \rightarrow 0$ K is estimated from the linear fit of C_p/T versus T^2 for $2 \text{ K} \leq T \leq 4 \text{ K}$, and it is found to increase linearly with H for low fields up to $H \approx 0.4 H_{c2}$. This behavior consistently supports a fully-gapped and almost isotropic superconducting order parameter.⁴⁷

The thermodynamic critical field $H_c(T)$ can be determined using $H_c(T) = \sqrt{-8\pi\Delta F}$ where ΔF is the free energy extracted from the specific heat in the superconducting state, $\Delta C_p = -Td^2(\Delta F)/dT^2$. The temperature dependence of $H_c(T)$ is shown in Fig. 7. Based on the BCS theory, $H_c(0)$ is derived from a fit to the temperature dependence of $H_c(T)$ for $T \rightarrow 0$ which is given by

$$\left(\frac{H_c(T)}{H_c(0)}\right)^2 = 1 - 2.12\beta \left(\frac{T}{T_c}\right)^2, \quad (4)$$

where the empirical parameter β is ~ 1 for the weak coupling limit but reduced with increasing e - ph coupling. The solid line in Fig. 7 is a best fit yielding $H_c(0) = 151.3(1) \text{ mT}$ and $\beta = 0.7933(3)$ indicating as well strong e - ph coupling. The deviation function, $D(t) = H_c(T)/H_c(0) - (1-t^2)$ with $t = T/T_c$ as well provides clear signatures for strong e - ph coupling. In the case of strongly e - ph coupled superconductors, $D(t)$ is positive and shows a broad maximum while the weak-coupling BCS curve exhibits a negative dip at $t^2 \approx 0.5$. As shown in the inset of Fig. 7, $D(t)$ for La_2C_3 passes through a maximum at $t^2 \approx 0.5$.

Based on the specific heat results for the superconducting states, we conclude that La_2C_3 is an s -wave, single gap superconductor with strong e - ph coupling. Recently, Harada *et al.* from ^{13}C nuclear-magnetic-resonance measurements suggested a multi-gap superconductivity for

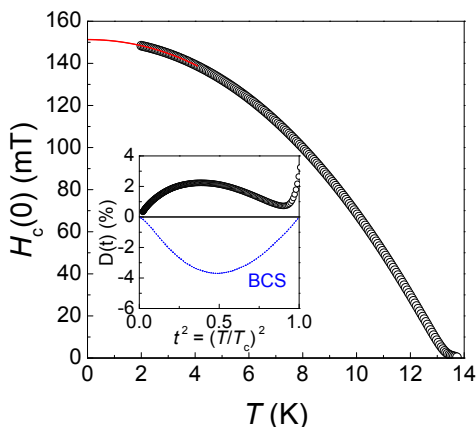


FIG. 7: (Color online) The temperature dependence of the thermodynamic critical field $H_c(T)$ estimated from the specific heat in the superconducting state. The solid (red) line is a best fit (see the text). The inset shows the deviation function, $D(t) = H_c(T)/H_c(0) - (1-t^2)$ with $t^2 = (T/T_c)^2$. The weak coupling BCS curve is also presented for comparison.

Y_2C_3 .⁴⁸ Since the Fermi surface consists of several sheets from hybridized La d and C p states, we cannot rule out such a possibility for La_2C_3 as well. However, as shown above, the specific heat for the superconducting state can be well explained in terms of a single superconducting gap. Usually, in a system where the d bands are hybridized with s or p bands, the disparity between the bands is reduced, and impurity scattering significantly smears out the two-gap superconductivity.^{49,50} Considering the polycrystalline nature of the sample, therefore, it is rather unlikely that, if any, two-gap superconductivity survives. Further studies are required to clarify the possible two-gap superconductivity in the sesquicarbide systems.

VI. UPPER CRITICAL FIELDS

Figure 8(a) shows the temperature dependence of the resistivity under different magnetic fields up to $H = 11 \text{ T}$. T_c is determined at 50% decrease from the normal state resistivity value and the transition width is taken as the temperature interval between 10% and 90% of the transition. In order to determine $H_{c2}(T)$ at low temperatures,

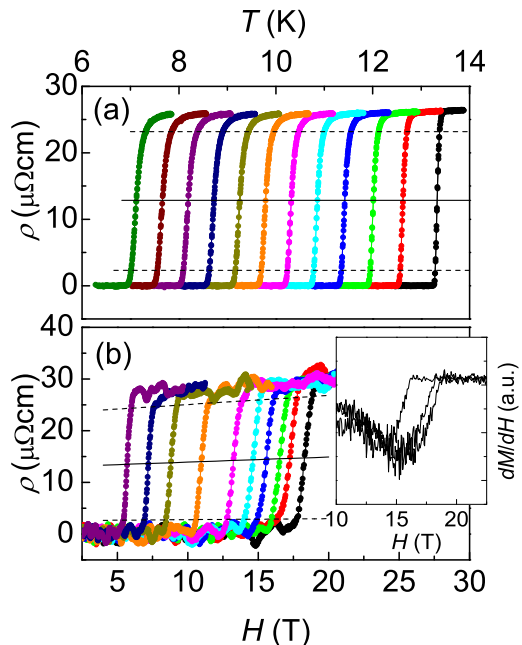


FIG. 8: (Color online) (a) Temperature dependence of the resistivity ($\rho(T)$) under magnetic fields from 0 to 11 T increasing by $\Delta H = 1 \text{ T}$, from right to left. (b) Magneto-resistivity ($\rho(H)$) at different temperatures at $T = 10, \dots, 2.4 \text{ K}$ from left to right. The (black) solid line presents 50% of the resistive transition, while two (black) dashed lines above and below denote 90% and 10% of the resistive transition. Note that $\rho(H)$ in (b) shows a slight positive magnetoresistance. The inset of (b) presents the first derivative of the magnetization versus field curve at $T = 4.2, 2.5,$ and 1.4 K , from left to right.

the magnetoresistance was measured up to ≈ 30 T at different temperatures from $T = 1.8$ to 10 K (Fig. 8(b)). The transition width remains almost unchanged down to low temperatures. As a consistency check we also carried out high field magnetization measurements at low temperatures. $H_{c2}(T)$ is determined as a kink of the first derivative of $M(H)$ (See the inset of Fig. 8).

The $H_{c2}(T)$ data obtained from the three different methods are compiled in Fig. 9. For comparison, we plotted the Werthammer-Helfand-Hohenberg (WHH) prediction for conventional superconductors.⁵¹ There is a clear deviation from the WHH behavior in the $H_{c2}(T)$ curve. This is in contrast to the previous report on the $H_{c2}(T)$ of La_2C_3 sample ($T_c \sim 11$ K), which followed the WHH prediction rather well. Such an enhancement of $H_{c2}(T)$ has been attributed to several different origins such as localization effects in highly disordered superconductors,⁵² anisotropy of the Fermi surface,⁵³ and strong e - ph coupling.^{54,55} First, considering disorder effects, the application of the magnetic field weakens the localization effects and thus reduces the Coulomb pseudopotential (μ^*). This in turn strengthens the superconductivity and leads to an enhancement of H_{c2} as the temperature decreases and larger fields have to be applied to drive the system into the normal state. Therefore, the enhancement of H_{c2} is closely linked to the negative magnetoresistance in the normal state.⁵² The positive magneto-resistance observed in La_2C_3 (See Fig. 8), however, indicates that the localization effects tend to be enhanced under high magnetic fields, which rules out the possibility of disorder-induced enhancement of H_{c2} . Secondly, when the FS is distorted from the spherical shape, an increase of H_{c2} becomes more pronounced due to an anisotropy in the FS.⁵³ Electron structure calculations for La_2C_3 unveil rather complex multisheets of the Fermi surface, similar to that of Y_2C_3 (*cf.* Fig. 5 in Ref. 8). A quantitative comparison between experiment and theory is beyond the scope of this work, but considering the distorted FS shape, the FS anisotropy will most likely contribute to the enhancement of H_{c2} at low temperatures. Note, however, that the previous report on $H_{c2}(T)$ for La_2C_3 ($T_c \sim 11$ K) with C deficiency showed good agreement with the WHH curve.¹² With C deficiency, the detailed FS can be modified, but the overall FS shape would be preserved, thus similar enhancement of H_{c2} at low temperatures is expected even for C-deficient samples with lower T_c . Therefore it seems that the FS anisotropy cannot be the only source for H_{c2} enhancement. Another possibility is strong e - ph coupling. When the e - ph coupling is in the strong coupling regime ($\lambda_{ph} > 1$), $H_{c2}(T)$ starts to deviate from the WHH curve and remains linear down to lower temperatures showing finally an upward curvature for higher e - ph coupling.⁵⁵ As shown in Fig. 9, $H_{c2}(T)$ for La_2C_3 shows an almost linear temperature dependence down to $\sim 0.2T_c$. From the specific heat studies, we already found evidence that the e - ph coupling is in the strong coupling regime, thus it will also affect the temperature dependence of H_{c2} for

La_2C_3 .

From an extrapolation, we obtained $H_{c2}(0) \approx 19$ T. Even though $H_{c2}(0)$ is much more enhanced than the WHH prediction, it is still clearly below the Pauli limit of $H_p(0) = \Delta(0)/2\sqrt{2}\mu_B = 1.83 k_B T_c \approx 24.5$ T for the weak coupling limit. Considering the strong e - ph coupling with enhanced $\Delta(0)/k_B T_c = 2.31 - 2.43$, $H_p(0)$ can be even higher up to ~ 32 T. Therefore, $H_{c2}(0) \approx 19$ T, well below the Pauli limit, indicates that H_{c2} is mainly determined by orbital depairing under magnetic fields. This result suggests that the possible effect due to non-centrosymmetry is not significant for H_{c2} as we will discuss below (see Sec. VII).

Based on the $H_{c2}(0)$ and $H_c(0)$ values, we estimated the superconducting parameters for La_2C_3 . According to the Ginzburg-Landau (GL) theory, the upper critical field $H_{c2}(0)$, the lower critical field $H_{c1}(0)$ and the thermodynamic critical field $H_c(0)$ can be described with the GL coherence length $\xi(0)$ and the GL parameter $\kappa(0) = \lambda(0)/\xi(0)$ according to

$$H_{c2}(0) = \frac{\Phi_0}{2\pi\xi(0)}, \quad (5)$$

$$H_{c1}(0) = \frac{H_c^2(0)}{H_{c2}(0)} [\ln \kappa(0) + 0.08], \quad (6)$$

$$H_c(0) = \frac{H_{c2}(0)}{\sqrt{2}\kappa(0)}, \quad (7)$$

where Φ_0 is the flux quantum. With $H_{c2}(0) = 19$ T and $H_c(0) = 151$ mT, we obtained $\xi(0) \approx 42$ Å and $\lambda(0) = 373$

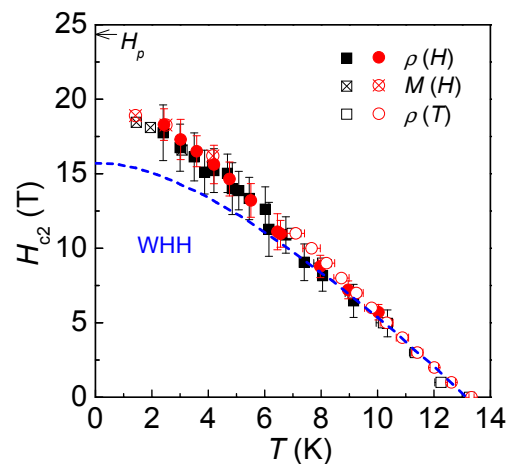


FIG. 9: (Color online) The temperature dependence of the upper critical field for La_2C_3 samples, S1 (square) and S3 (circle), estimated from $\rho(H)$ (filled symbols), $M(H)$ (crossed symbols), and $\rho(T)$ (open symbols) measurements. For comparison, the Werthammer-Helfand-Hohenberg curve with the Maki parameter $\alpha = 0$ and the spin-orbit scattering $\lambda_{SO} = 0$ (see Ref. 51) is presented with (blue) dashed line. The Pauli limit H_p is indicated by the arrow.

nm. The GL parameter, $\kappa(0)$ is ≈ 90 , indicating type-II superconductivity. Similar values have also been reported for the 14 K phase of Y_2C_3 ($T_c = 13.9$ K): $H_{c1}(0) = 3.5$ mT, $\lambda(0) = 430$ nm, $H_{c2} = 24.7$ T, and $\xi(0) = 36$ Å.⁵⁶

VII. DISCUSSION

First we briefly discuss the effect of non-centrosymmetry in La_2C_3 . There have been several characteristic features reported concerning the effect of the lack of centrosymmetry on the superconducting properties : (1) enhancement of $H_{c2}(0)$ above the Pauli limit (2) presence of a line node in the superconducting gap parameters. Furthermore, it has been suggested that a description of the superconducting properties should at least include two bands due to the non-centrosymmetry in rare earth sesquicarbides.²³ Our electronic structure calculations confirm the splitting in the electronic bands near E_F indicating that the spin degeneracy is lifted due to the sizable asymmetric spin-orbit coupling.

However, even though $H_{c2}(0)$ is clearly enhanced, it does not exceed the paramagnetic limit (Fig. 9). The specific heat at low temperatures also reveals that the superconducting gap in La_2C_3 has an isotropic s -wave symmetry. Therefore the effect of the non-centrosymmetry appears to be not significant in La_2C_3 . Note that the band splitting with respect to the superconducting transition temperature is much smaller for La_2C_3 than in other non-centrosymmetric superconductors (See Table II). In $\text{Li}_2\text{Pd}_3\text{B}$ where the band splitting due to non-centrosymmetry is comparable with that of La_2C_3 , conventional BCS type behavior with the isotropic superconducting gap has been found from penetration depth measurements using muon-spin-rotation experiments.⁵⁹ Therefore for La_2C_3 , the asymmetric spin-orbit coupling appears to be not strong enough to induce a significant effect on the superconducting properties. In this respect, it would be very interesting to study heavier rare earth metal carbides such as Lu_2C_3 ($T_c \approx 15$ K)⁶⁰ and Th_2C_3 ($T_c \approx 4$ K).⁴¹

For e - ph coupled superconductors, Carbotte⁶¹ has proposed that the characteristic thermodynamic quantities follow empirical formulas which can be described by one adjustable parameter, $x = \omega_{ln}/T_c$ where ω_{ln} is the logarithmic averaged phonon frequency:

rithmic averaged phonon frequency:

$$\frac{2\Delta(0)}{k_B T_c} = 3.53 \left[1 + 12.5x^{-2} \ln \frac{x}{2} \right], \quad (8)$$

$$\frac{\Delta C_p(T_c)}{\gamma_N T_c} = 1.43 \left[1 + 53x^{-2} \ln \frac{x}{3} \right], \quad (9)$$

$$\frac{\Delta C_p(T) - \Delta C_p(T_c)}{\gamma_N T_c - \gamma_N T} = -3.77 \left[1 + 117x^{-2} \ln \frac{x}{2.9} \right], \quad (10)$$

$$\frac{\gamma_N T_c^2}{H_c^2(0)} = 0.168 \left[1 - 12.2x^{-2} \ln \frac{x}{3} \right], \quad (11)$$

$$\frac{H_c(0)}{dH_c(T)/dT|_{T_c} T_c} = 0.576 \left[1 - 13.4x^{-2} \ln \frac{x}{3.5} \right]. \quad (12)$$

This analysis has been successfully applied to various metal-alloy superconductors,⁶¹ and also to other recently discovered carbon-contained superconductors such as borocarbides^{62,63} and MgCNi_3 .⁶⁴

Figure 10 shows the thermodynamic quantities with variation of $x = \omega_{ln}/T_c$ according to Eqs. (8)-(12). The

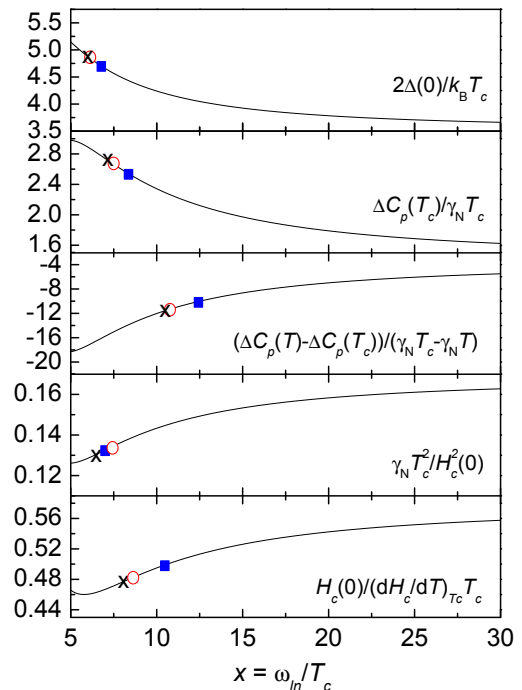


TABLE II: Energy splitting of the bands at E_F (ΔE) and T_c for several non-centrosymmetric superconductors.

	ΔE (meV)	$\Delta E/k_B T_c$	T_c (K)	Ref.
La_2C_3	20 - 30	~ 20	13.4	this work
CePt_3Si	50 - 200	> 1000	0.75	19
$\text{Cd}_2\text{Re}_2\text{O}_7$	~ 70	~ 700	~ 1	57
$\text{Li}_2\text{Pt}_3\text{B}$	~ 200	> 1000	~ 2	58
$\text{Li}_2\text{Pd}_3\text{B}$	20 - 50	$> 35 - 85$	~ 7	58

FIG. 10: (Color online) Several thermodynamic quantities as a function of the logarithmic averaged phonon frequency (solid line) according to Eqs. (8)-(12). The thermodynamic quantities estimated from the specific heat data for the samples are indicated with (red) open circles for S1, (black) crosses for S2 and (blue) filled squares for S3.

measured values extracted from the C_p data are also plotted onto the empirical curves. Each thermodynamic quantity provide a value for $x = \omega_{ln}/T_c$ as indicated for three La_2C_3 samples (S1-S3) in Fig. 10. From five x 's and $T_c = 13.4$ K, we obtain a mean value $\omega_{ln} = 109$ K \pm 24 K, 101 K \pm 24 K, and 121 K \pm 32 K for the sample S1, S2, and S3, respectively. Averaging all ω_{ln} 's for the samples we conclude on $\omega_{ln} = 110$ K \pm 27 K. This ω_{ln} value is only $\sim 30\%$ of the Debye temperature, $\omega_D \approx 350$ K. The Debye frequency is determined only from the phonon DOS profile, $F(\omega)$, while ω_{ln} results from a weighting by the e - ph coupling function $\alpha^2(\omega)$. Such a reduced ω_{ln} value compared to ω_D indicates the importance of the low energy phonon modes for the superconductivity. The deviation of the normal state C_p from the Debye T^3 law (See. Fig 4) supports the presence of the low-lying Einstein phonon modes.

From *ab-initio* calculations for Y_2C_3 , the frequencies of the full symmetry Raman modes are estimated to be 175 cm^{-1} for a Y dominated mode and 1442 cm^{-1} for an almost pure C-C bond stretching mode.⁸ The relevant phonon modes for the superconductivity, therefore, are the La dominated phonon modes rather than the high frequency C-C bond stretching modes. From simple conversion based on the atomic mass difference between La and Y, we can estimate the frequency of the La dominated Raman mode to be ~ 140 cm^{-1} . In comparison with $\omega_{ln} \approx 76$ $\text{cm}^{-1} \pm 15$ cm^{-1} , this phonon frequency is somewhat higher. However, since the lattice constant of La_2C_3 is larger than that of Y_2C_3 , the interatomic forces are expected to be somewhat weaker for La_2C_3 . The estimated frequency of the La dominated phonon mode, therefore, is rather overestimated, and it can be reduced

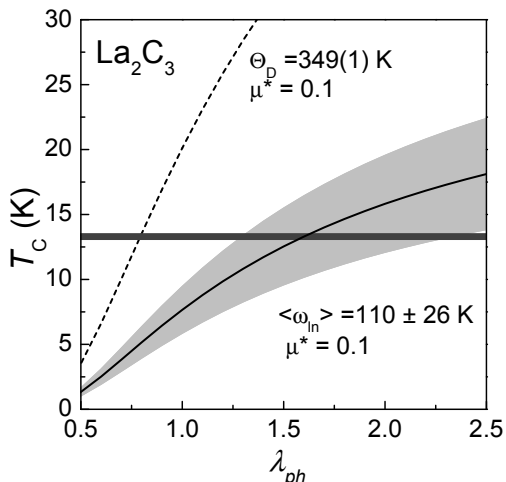


FIG. 11: The calculated T_c from the modified McMillan formula (solid line) as a function of the e - ph coupling constant, λ_{ph} . The borders of the shaded (grey) areas represent the results obtained for the upper and lower bounds of ω_{ln} . For comparison, we also plot the calculated T_c from the original McMillan formula with dashed line. The horizontal (dark grey) solid line denotes the measured T_c .

and come closer to the ω_{ln} . Recent *ab-initio* calculations for Y_2C_3 also reported that most of the e - ph coupling emerges from the low frequency Y related phonon modes, not from the high frequency C-C phonon modes.⁸

Other relevant phonon modes for superconductivity in La_2C_3 could be the tilting vibrations of the C-C dimer. For AC_2 ($A = \text{Ca}, \text{Sr}, \text{and Ba}$) containing the C-C dimers inside the octahedral metal atom cage, it has been shown that the binding of the C-C dimer to the surrounding octahedral metal atom cage is weak, thus allowing a structural transition from tetragonal to a cubic phase at high temperatures as well as several modifications of the C-C dimer structure at low temperatures.⁶⁶ Raman scattering studies on rare-earth carbide halides also showed that the frequency of the C-C tilting modes is ~ 400 cm^{-1} , much lower than the stretching modes with a frequency of ~ 1590 cm^{-1} .³⁵ Compared to the octahedral metal atom cages, the size of a bisphenoid La cage is larger, thus the binding of the C-C dimer to the La cage could be even weaker. Consequently the tilting modes of the C-C dimer in La_2C_3 are expected to have lower frequencies, which can allow sizable contribution to e - ph coupling. Further studies on the C-C dimer tilting modes *e.g.* Raman scattering experiments or *ab-initio* calculations are highly desirable.

Finally we estimate the e - ph coupling constant for La_2C_3 . Based on the Sommerfeld coefficient and the electronic structure calculation, we obtain λ_{ph} from the determination of γ_N using the equation $\gamma_N = (2\pi^2 k_B^2/3)N(E_F)(1+\lambda_{ph})$. From the DOS calculations for the 2% C deficient compounds, we take $N(E_F) = 1.75$ states/eV f.u. Using $\gamma_N = 10.6$ mJ/mol K², the estimated λ_{ph} is 1.4 indicating that the La_2C_3 clearly belongs to the strong coupling regime.

In Fig. 11 we plot the calculated T_c from the modified McMillan formula,

$$T_c = \frac{\omega_{ln}}{1.2} \exp \left[\frac{-1.04(1 + \lambda_{ph})}{\lambda_{ph} - (1 + 0.62\lambda_{ph})\mu^*} \right], \quad (13)$$

with the measured $T_c = 13.4$ K (grey horizontal line). For comparison we also plot the calculated T_c from the original McMillan formula.⁶⁷ In both cases, the Coulomb pseudopotential μ^* is fixed to 0.1. With the original McMillan formula assuming the effective phonon frequency to be the same as the Debye frequency, we found that the measured T_c is reproduced with weak e - ph coupling, $\lambda_{ph} \sim 0.75$. However such a weak coupling cannot reconcile with the results of specific heat and upper critical fields as discussed above. If we use the logarithmic averaged phonon frequency ω_{ln} in the modified McMillan formula, Eq. (13), a large value of λ_{ph} is necessary to reproduce the measured T_c . Because of the relatively large error for the calculated T_c from the modified McMillan formula due to the reduced accuracy for determining ω_{ln} , it is difficult to determine the λ_{ph} value precisely. However it is obvious that λ_{ph} is larger than 1.3, which is in good agreement with the estimate from the comparison of the Sommerfeld coefficient.

In conclusion, specific heat and upper critical field studies were performed on the sesquicarbide superconductor La_2C_3 together with neutron powder diffraction as well as electronic structure calculations. The main conclusions are the followings. (i) The density of states near the E_F is very sensitive to a small C deficiency in the sample, which provides an explanation for the wide scatter of T_c 's and superconducting properties observed in the previous reports. (ii) The temperature and magnetic field dependence of the specific heat is consistent with a single gap s -wave BCS superconductor. (iii) The logarithmic averaged phonon frequency for the superconductivity is quite low suggesting the importance of low energy phonon modes for the superconductivity. (iv) Even though the band splitting due to the non-centrosymmetry in the structure and the spin-orbit coupling is clearly confirmed by the electronic structure cal-

culations, its effect seems not sizable enough to cause exotic superconducting properties as observed in other non-centrosymmetric superconductors. To conclude, all of the summarized features suggest that La_2C_3 is a strongly coupled BCS-type superconductor with an isotropic s -wave superconducting gap.

Acknowledgments

The authors acknowledge stimulating discussions with A. Das and O. Dolgov. We thank E. Brücher and G. Siegle for expert experimental assistance. Part of this work has been supported by EuroMagNET under the EU contract RII3-CT-2004-506239.

-
- ¹ J. Nagamitsu, N. Nakagawa, T. Muranaka, and J. Akimitsu, *Nature* **410**, 63 (2001).
 - ² T. E. Weller, M. Ellerby, S. S. Saxena, R. P. Smith, and N. T. Skipper, *Nature Physics* **1**, 39 (2005); N. Emery, C. Hérod, M. d'Astuto, V. Garcia, Ch. Bellin, J.F. Marêché, P. Lagrange, and G. Loupiau, *Phys. Rev. Lett.* **95**, 087003 (2005).
 - ³ K. Shimizu, H. Kimura, D. Takao, and K. Amaya, *Nature* **419**, 597 (2002); V. V. Struzhkin, M. I. Erements, W. Gan, H.-K. Mao, and R. J. Hemley, *Science* **298**, 1213 (2002); S. Deemyad and J. S. Schilling, *Phys. Rev. Lett.* **91**, 167001 (2003).
 - ⁴ Deepa Kasinathan, J. Kunes, A. Lazicki, H. Rosner, C. S. Yoo, R. T. Scalettar, and W. E. Pickett, *Phys. Rev. Lett.* **96**, 047004 (2006); G. Profeta, C. Franchini, N. N. Lathiotakis, A. Floris, A. Sanna, M. A. L. Marques, M. Lüders, S. Massidda, E. K. U. Gross, and A. Continenza, *ibid.* **96**, 047003 (2006).
 - ⁵ W. E. Pickett, cond-mat/0603428; cond-mat/0603482 (unpublished).
 - ⁶ N. W. Ashcroft, *Phys. Rev. Lett.* **21**, 1748 (1968).
 - ⁷ M. C. Krupka, A. L. Giorgi, N. H. Krikorian, and E. G. Szklarz, *J. Less-Common Met.* **19**, 113 (1969).
 - ⁸ D. J. Singh and I. I. Mazin, *Phys. Rev. B* **70**, 052504 (2004).
 - ⁹ G. Amano, S. Akutagawa, T. Muranaka, Y. Zenitani, and J. Akimitsu, *J. Phys. Soc. Jpn.* **73**, 530 (2004).
 - ¹⁰ T. Nakane, T. Mochiku, H. Kito, M. Nagao, J. Itoh, H. Kumakura, and Y. Takano, *Appl. Phys. Lett.* **84**, 2859 (2004).
 - ¹¹ I. R. Shein and A. L. Ivanovskii, cond-mat/0312391.
 - ¹² T. L. Francavilla and F. L. Carter, *Phys. Rev. B* **14**, 128 (1976).
 - ¹³ A. Simon and Th. Gulden, *Z. Anorg. Allg. Chem.* **630**, 2191 (2004).
 - ¹⁴ R. K. Kremer and A. Simon, *Curr. Appl. Phys.* **4**, 563 (2004).
 - ¹⁵ Th. Gulden, PhD Thesis, Universität Stuttgart, 1997.
 - ¹⁶ J. S. Kim, R. K. Kremer, O. Jepsen, A. Simon, *Curr. Appl. Phys.* **6** 897 (2006).
 - ¹⁷ X. Wang, I. Loa, K. Syassen, R. K. Kremer, A. Simon, M. Hanfland, and K. Ahn, *Phys. Rev. B* **72**, 064520 (2005).
 - ¹⁸ E. Bauer, G. Hilscher, H. Michor, Ch. Paul, E.W. Scheidt, A. Griбанov, Yu. Seropegin, H. Noël, M. Sigrist, and P. Rogl, *Phys. Rev. Lett.* **92**, 027003 (2004).
 - ¹⁹ K. V. Samokhin, E. S. Zijlstra, and S. K. Bose, *Phys. Rev. B* **69**, 094514 (2004).
 - ²⁰ K. Izawa, Y. Kasahara, Y. Matsuda, K. Behnia, T. Yasuda, R. Settai, and Y. Onuki, *Phys. Rev. Lett.* **94**, 197002 (2005).
 - ²¹ I. Bonalde, W. Brämer-Escamilla, and E. Bauer, *Phys. Rev. Lett.* **94**, 207002 (2005).
 - ²² H. Q. Yuan, D. F. Agterberg, N. Hayashi, P. Badica, D. Vandervelde, K. Togano, M. Sigrist, and M. B. Salamon, *Phys. Rev. Lett.* **97**, 017006 (2006).
 - ²³ It has been suggested that Th doping in R_2C_3 ($R = Y$ and La) will enhance the effect of the non-centrosymmetry in the structure because of the heavy atomic mass of Th [Ivan A. Sergienko, *Physica B* **356-361**, 581 (2005)].
 - ²⁴ F. H. Spedding, K. A. Gschneidner jr., A. H. Daane, *Trans. AIME* **215**, 192 (1959).
 - ²⁵ J. Rodriguez-Carvajal, FULLPROF, version June 2005, ILL (unpublished).
 - ²⁶ M. Atoji, K. Gschneidner Jr., A. H. Daane, R. E. Rundle, and F. H. Spedding, *J. Am. Chem. Soc.* **80**, 1804 (1958).
 - ²⁷ M. Atoji and D. E. Williams, *J. Chem. Phys.* **35**, 1960 (1961).
 - ²⁸ V. I. Novokshonov, E. P. Khlybov, V. V. Evdokimova, *Russian Metallurgy* **3**, 167 (1980).
 - ²⁹ T. G. Amos, Q. Huang, J. W. Lynn, T. He and R. J. Cava, *Sol. State Comm.* **121**, 73 (2002).
 - ³⁰ P. J. T. Joseph and P. P. Singh, *Phys. Rev. B* **72**, 064519 (2005).
 - ³¹ M. D. Johannes and W. E. Pickett, *Phys. Rev. B* **70**, 060507(R) (2004).
 - ³² A. Wälte, G. Fuchs, K.-H. Müller, S.-L. Drechsler, K. Nenkov, and L. Schultz, *Phys. Rev. B* **72**, 100503(R) (2005) and references therein.
 - ³³ A. Simon, Hj. Mattausch, R. Eger, and R. K. Kremer, *Handbook of the Physics and Chemistry of Rare Earths* **15**, (ed. K. A. Gschneidner jr., L. Eyring), Elsevier Science Publ., Amsterdam, 191 (1991).

- ³⁴ A. Simon, A. Yoshiasa, M. Bäcker, R. W. Henn, R. K. Kremer, H. J. Mattausch, and C. Felser, *Z. anorg. allg. Chem.* **622**, 123 (1996).
- ³⁵ R. W. Henn, T. Strach, R. K. Kremer, and A. Simon, *Phys. Rev. B* **58**, 14364 (1998).
- ³⁶ J. Li and R. Hoffmann, *Chem. Mater.* **1**, 83 (1989).
- ³⁷ P. Blaha, K. Schwarz, G. K. H. Madsen, D. Kvasnicka, and J. Luitz, *Wien2k, an Augmented Plane Wave+Local Orbitals Program for Calculating Crystal Properties* (Karlheinz Schwarz, Techn. Universität Wien, Austria), ISBN 3-9501031-1-2.
- ³⁸ J. P. Perdew, K. Burke and M. Ernzerhof, *Phys. Rev. Lett.* **77**, 3865 (1996).
- ³⁹ In the calculations, we set $RK_{\max} = 5.5$, $l = 12$ and $G_{\max} = 18$. The muffin-tin radii of $2.5 a_0$ and $1.14 a_0$ were chosen for La and C, respectively. For the spin-orbit calculation, the states up to 10 Ry are included in the second-variation diagonalization of the spin-orbit Hamiltonian.
- ⁴⁰ I. A. Sergienko and S. H. Curnoe, *Phys. Rev. B* **70**, 214510 (2004).
- ⁴¹ A. L. Giorgi, E. G. Sklarz, N. H. Krikorian, and M. C. Krupka, *J. Less-Common Met.* **22**, 131, (1970).
- ⁴² K. Ahn, B. I. Gipson, R. K. Kremer, H. Mattausch, A. Stolovits, and A. Simon, *Int. J. Self-Propag. High-Temp. Synth.* **103**, 5446 (1999).
- ⁴³ A. L. Giorgi, E. G. Sklarz, M. C. Krupka, T. C. Wallace, and N. H. Krikorian, *J. Less-Common Met.* **14**, 247, (1968).
- ⁴⁴ Y. Muto, N. Toyota, K. Noto, K. Akutsu, M. Isino, and T. Fukase, *J. Low Temp. Phys.* **34**, 617 (1979).
- ⁴⁵ J. S. Kim, R. K. Kremer, L. Boeri, and F. S. Razavi, *Phys. Rev. Lett.* **96**, 217002 (2006).
- ⁴⁶ H. Padamsee, J. E. Neighbor, and C. A. Shiffman, *J. Low Temp. Phys.* **12**, 387 (1973).
- ⁴⁷ N. Nakai, P. Miranović, M. Ichioka, and K. Machida, *Phys. Rev. B* **70**, 100503(R) (2004).
- ⁴⁸ A. Harada, S. Akutagawa, Y. Miyamichi, H. Mukuda, Y. Kitaoka, and J. Akimitsu, cond-mat/0612578 (2006).
- ⁴⁹ I. I. Mazin, O. K. Andersen, O. Jepsen, O. V. Dolgov, J. Kortus, A. A. Golubov, A. B. Kuzmenko, and D. van der Marel, *Phys. Rev. Lett.* **89** 107002 (2002).
- ⁵⁰ J. Kortus, O. V. Dolgov, R. K. Kremer, and A. A. Golubov, *Phys. Rev. Lett.* **94**, 027002 (2005).
- ⁵¹ N. R. Werthamer, E. Helfand, and P. C. Hohenberg, *Phys. Rev.* **147**, 295 (1966).
- ⁵² L. Coffey, K. A. Muttalib, and K. Levin, *Phys. Rev. Lett.* **52**, 783 (1984); Liam Coffey, K. Levin, and K. A. Muttalib, *Phys. Rev. B* **32**, 4382 (1985).
- ⁵³ T. Kita and M. Arai, *Phys. Rev. B* **70**, 224522 (2004).
- ⁵⁴ F. Marsiglio and J. P. Carbotte, *Phys. Rev. B* **41**, 8765 (1990).
- ⁵⁵ L. N. Bulaevskii, O. V. Dolgov, and M. O. Ptitsyn, *Phys. Rev. B* **38**, 11290 (1988).
- ⁵⁶ J. Akimitsu, S. Akutagawa, K. Kawashima and T. Muranaka, *Prog. Theor. Phys. Supplement No.* **159**, 326 (2005); S. Akutagawa and J. Akimitsu, *Sci. Technol. Adv. Mater.* **7**, 2 (2006).
- ⁵⁷ R. Eguchi, T. Yokoya, T. Baba, M. Hanawa, Z. Hiroi, N. Kamakura, Y. Takata, H. Harima, and S. Shin, *Phys. Rev. B* **66**, 012516 (2002).
- ⁵⁸ K.-W. Lee and W. E. Pickett, *Phys. Rev. B* **72**, 174505 (2005).
- ⁵⁹ R. Khasanov, I. L. Landau, C. Baines, F. La Mattina, A. Maisuradze, K. Togano, and H. Keller, *Phys. Rev. B* **73**, 214528 (2006).
- ⁶⁰ L. F. Vereshchagin *et al.*, *Fiz. tverdogo tela* **20**, 3109 (1978).
- ⁶¹ J. P. Carbotte, *Rev. Mod. Phys.* **62** 1027 (1990).
- ⁶² S. Manalo, H. Michor, M. El-Hagary, G. Hilscher, and E. Schachinger, *Phys. Rev. B* **63**, 104508 (2001).
- ⁶³ H. Michor, R. Krendelsberger, G. Hilscher, E. Bauer, C. Dusek, R. Hauser, L. Naber, D. Werner, P. Rogl, and H. W. Zandbergen, *Phys. Rev. B* **54**, 9408 (1996).
- ⁶⁴ A. Wälte, G. Fuchs, K.-H. Müller, A. Handstein, K. Nenkov, V. N. Narozhnyi, S.-L. Drechsler, S. Shulga, L. Schultz, and H. Rosner, *Phys. Rev. B* **70**, 174503 (2004).
- ⁶⁵ W. L. McMillan, *Phys. Rev.* **167**, 331 (1968); P. B. Allen and R. C. Dynes, *Phys. Rev. B* **12**, 905 (1975).
- ⁶⁶ M. Knapp and U. Ruschewitz, *Chem. Eur. J.* **2001**, 874 (2001) and the references therein.
- ⁶⁷ The only difference of the original McMillan formular from Eq. (13) is that the coefficient $\omega_{ln}/1.2$ is replaced by $\Theta_D(0)/1.45$. See Ref. 65.